

# Soliton interactions in the Sasa-Satsuma equation on the continuous wave background

Tao Xu<sup>1</sup> and Min Li<sup>2</sup>

1. *College of Science, China University of Petroleum, Beijing 102249, China.*

*E-mail: xutao@cup.edu.cn.*

2. *Department of Mathematics and Physics, North China Electric*

*Power University, Beijing 102206, China. E-mail: micheller85@126.com.*

## Abstract

Via the successively-iterated Darboux transformation, we obtain a general family of soliton solutions for the Sasa-Satsuma equation (SSE) starting from a nonzero seed. It is found that the SSE admits both the anti-dark and Mexican-hat solitons on the continuous wave background. Also, we reveal that the resonant and elastic soliton interactions as well as various combinations of such two fundamental interactions can occur in the SSE. In addition, we show that the interacting soliton may exchange its energy with the background, which results in an anti-dark soliton changing into a Mexican-hat one, or a Mexican-hat soliton into an anti-dark one. Our results enrich the knowledge of soliton interactions in the (1+1)-dimensional integrable equations with a single field.

PACS numbers: 05.45.Yv, 02.30.Ik

*Introduction.* — It has been found that the (2+1)-dimensional integrable systems (e.g., the Kadomtsev-Petviashvili II equation [1–3]) admit a large variety of soliton interaction patterns in the spatial plane at a given time. The amplitudes, directions and number of incoming solitons are in general different from those of the outgoing ones [1, 2]. Moreover, the asymptotic solitons interact in the near-field region to form intermediate solitons and various web-like structures via the “X” and “Y”-junctions which, respectively, corresponds to the fundamental elastic and resonant

interactions [2, 3]. However, the soliton interactions are usually thought to be elastic in the (1+1)-dimensional integrable equations [(1+1)-DIEs] with a single field, that is, the amplitudes, velocities and number of interacting solitons are the same before and after interactions except for the phase shifts [4].

In this Letter, we are devoted to studying the soliton interaction dynamics underlying in the Sasa-Satsuma equation (SSE) [5]:

$$i u_z + \frac{1}{2} u_{tt} + |u|^2 u + i \varepsilon [u_{ttt} + 6 |u|^2 u_t + 3 u (|u|^2)_t] = 0, \quad (1)$$

which is an integrable higher-order nonlinear Schrödinger equation. The SSE can be used to approximately describe the femtosecond pulse propagation in the monomode optical fibers, and the last three terms in Eq. (1) stand for the third-order dispersion, self-steepening and stimulated Raman scattering (SRS), respectively [6]. Over the past two decades, many integrable properties of the SSE have been detailed, like the inverse scattering transform scheme [5, 7], bilinear representation [8], Painlevé property [9], conservation laws [10], nonlocal symmetries [11], squared eigenfunctions [12], Bäcklund transformation [13] and Darboux transformation (DT) [14, 15].

With the presence of the SRS term, the SSE has abundant solitonic behavior [5, 7, 8, 15–19]. Under the vanishing boundary condition (VBC), apart from the single-hump soliton [5, 16], Eq. (1) possesses the double-hump soliton which behaves like two in-phase solitons propagating with the same velocity and fixed separation [5, 7], and the multi-hump breather with the oscillating structure in a periodic fashion during the propagation [7, 8]. Under the non-vanishing boundary condition, Eq. (1) admits the anti-dark (AD) soliton which exhibits the form of a bright pulse on the continuous wave (CW) pedestal (i.e., it is like a dark soliton with reverse sign amplitude) [17, 18], the “W”-shaped soliton which takes the shape of the letter “W” within the CW background [17], and the double-hole dark soliton displaying two holes which are beneath the background and have a fixed separation [18, 19]. In addition, Eq. (1) has also been found to have the the unusual double-peak rogue wave [20] and “W”-shaped rogue wave [21], which are both generated by the modulationally unstable plane wave.

As a matter of fact, beyond what we have already known, there are considerable complicated soliton interaction phenomena in Eq. (1). Even for Eq. (1) with the VBC, the shape-changing interactions can occur between the soliton and breather, that is, one soliton may change into a

breather upon interaction with a breather, or one breather into a soliton when interacting with another breather [15]. In the following, we will use the DT method [22] to construct a general family of soliton solutions of Eq. (1) starting from a nonzero seed, and reveal that Eq. (1) can exhibit the resonant (inelastic) interaction, elastic interaction and various combinations of such two fundamental interactions. To our knowledge, it is the first time that such abundant soliton interactions have been found in the (1+1)-DIE with a single field.

*N-th iterated solutions via the Darboux transformation.* — To begin with, we introduce the transformations  $u(t, z) = p(\eta, \xi) e^{i(\frac{t}{6\varepsilon} - \frac{z}{108\varepsilon^2})}$ ,  $\eta = t - \frac{z}{12\varepsilon}$  and  $\xi = \varepsilon z$ . As a result, Eq. (1) can be simplified as the complex modified Korteweg-de Vries equation [5]:

$$p_\xi + p_{\eta\eta\eta} + 6|p|^2 p_\eta + 3(|p|^2)_\eta p = 0, \quad (2)$$

which admits the Lax pair

$$\Psi_\eta = \begin{pmatrix} \lambda & \mathbf{P} \\ -\mathbf{P}^\dagger & -\lambda \mathbf{E}_2 \end{pmatrix} \Psi, \quad (3a)$$

$$\Psi_\xi = \begin{pmatrix} -4\lambda^3 - 2\lambda\mathbf{P}\mathbf{P}^\dagger & -4\lambda^2\mathbf{P} - 2\lambda\mathbf{P}_\eta \\ +\mathbf{P}\mathbf{P}_\eta^\dagger - \mathbf{P}_\eta\mathbf{P}^\dagger & -\mathbf{P}_{\eta\eta} - 2\mathbf{P}\mathbf{P}^\dagger\mathbf{P} \\ 4\lambda^2\mathbf{P}^\dagger - 2\lambda\mathbf{P}_\eta^\dagger & 4\lambda^3\mathbf{E}_2 + 2\lambda\mathbf{P}^\dagger\mathbf{P} \\ +\mathbf{P}_\eta^\dagger + 2\mathbf{P}^\dagger\mathbf{P}\mathbf{P}^\dagger & +\mathbf{P}^\dagger\mathbf{P}_\eta - \mathbf{P}_\eta^\dagger\mathbf{P} \end{pmatrix} \Psi, \quad (3b)$$

where  $\mathbf{P} = (p, p^*)$ ,  $\Psi = (\psi_1, \psi_2, \psi_3)^T$  is the eigenfunction,  $\lambda$  is the spectral parameter,  $\mathbf{E}_2$  is the  $2 \times 2$  identity matrix, and the dagger denotes the Hermitian conjugate.

In Ref. [15], we have presented the N-th successively-iterated DT on Lax pair (3a) and (3b), which makes it easy to uniformly represent the iterated solutions in terms of some determinant. Here, we implement the DT algorithm starting from the seed solution  $u = \rho e^{i(\frac{t}{6\varepsilon} - \frac{z}{108\varepsilon^2} + \phi)}$  (i.e.,  $p = \rho e^{i\phi}$ ,  $\rho > 0$  and  $\phi$  are both real constants), and obtain the iterated solutions in the following multi-component determinant form:

$$u[N] = e^{i(\frac{t}{6\varepsilon} - \frac{z}{108\varepsilon^2})} \left( \rho e^{i\phi} - 2 \frac{\tau_{N+1, N-1, N}}{\tau_{N, N, N}} \right), \quad (4a)$$

$$u^*[N] = e^{-i(\frac{t}{6\varepsilon} - \frac{z}{108\varepsilon^2})} \left( \rho e^{-i\phi} - 2 \frac{\tau_{N+1, N, N-1}}{\tau_{N, N, N}} \right), \quad (4b)$$

with

$$\tau_{J,K,L} = \begin{pmatrix} \mathbf{F}_{N \times J} & -\mathbf{G}_{N \times K} & -\mathbf{H}_{N \times L} \\ \mathbf{F}_{N \times J}^* & -\mathbf{H}_{N \times K}^* & -\mathbf{G}_{N \times L}^* \\ \mathbf{G}_{N \times J}^* & \mathbf{F}_{N \times K}^* & \mathbf{0} \\ \mathbf{H}_{N \times J} & \mathbf{F}_{N \times K} & \mathbf{0} \\ \mathbf{H}_{N \times J}^* & \mathbf{0} & \mathbf{F}_{N \times L}^* \\ \mathbf{G}_{N \times J} & \mathbf{0} & \mathbf{F}_{N \times L} \end{pmatrix}, \quad (5)$$

where  $J + K + L = 6N$ ,  $\mathbf{F}_{N \times J} = (\lambda_k^{m-1} f_k)_{1 \leq k \leq N, 1 \leq m \leq J}$ ,  $\mathbf{G}_{N \times K} = [(-\lambda_k)^{m-1} g_k]_{1 \leq k \leq N, 1 \leq m \leq K}$ ,  $\mathbf{H}_{N \times L} = [(-\lambda_k)^{m-1} h_k]_{1 \leq k \leq N, 1 \leq m \leq L}$ , the vector function  $(f_k, g_k, h_k)^T$  corresponds to the solution of Lax pair (3a) and (3b) with  $p = \rho e^{i\phi}$  and  $\lambda = \lambda_k$  ( $1 \leq k \leq N$ ):

$$\begin{pmatrix} f_k \\ g_k \\ h_k \end{pmatrix} = \begin{pmatrix} e^{\frac{i\phi}{2}} (\alpha_k e^{\theta_k(t,z)} + \beta_k e^{-\theta_k(t,z)}) \\ -e^{-\frac{i\phi}{2}} \left( \frac{\rho \alpha_k}{\chi_k} e^{\theta_k(t,z)} + \frac{\rho \beta_k}{\chi_k} e^{-\theta_k(t,z)} - \gamma_k e^{-\omega_k(t,z)} \right) \\ -e^{\frac{3i\phi}{2}} \left( \frac{\rho \alpha_k}{\chi_k} e^{\theta_k(t,z)} + \frac{\rho \beta_k}{\chi_k} e^{-\theta_k(t,z)} + \gamma_k e^{-\omega_k(t,z)} \right) \end{pmatrix}, \quad (6)$$

with  $\theta_k(t, z) = \chi_k \left[ t - \frac{z}{12\varepsilon} - 4(\lambda_k^2 + \rho^2) \varepsilon z \right]$ ,  $\omega_k(t, z) = \lambda_k \left( t - \frac{z}{12\varepsilon} - 4\lambda_k^2 \varepsilon z \right)$ ,  $\chi_k = \sqrt{\lambda_k^2 - 2\rho^2}$ ,  $\chi_k^+ = \lambda_k + \sqrt{\lambda_k^2 - 2\rho^2}$ ,  $\chi_k^- = \lambda_k - \sqrt{\lambda_k^2 - 2\rho^2}$ ,  $\alpha_k$ ,  $\beta_k$  and  $\gamma_k$  being nonzero complex constants.

We point that the determinant representation in (5) can provide an algebraic basis for us to analyze the asymptotic behavior of the soliton solutions [23] on the CW background. In order to derive the soliton solutions, we require that  $\chi_k$ 's ( $1 \leq k \leq N$ ) are all real numbers, that is,  $\text{Im}(\lambda_k) = 0$  and  $|\lambda_k| > \sqrt{2}\rho$ . For convenience of our analysis, we introduce the following notations: (a)  $\mu_k^{(1)} = \alpha_k^* \beta_k - \alpha_k \beta_k^*$ ,  $\mu_k^{(2)} = \alpha_k^* \gamma_k + \alpha_k \gamma_k^*$  and  $\mu_k^{(3)} = \beta_k^* \gamma_k + \beta_k \gamma_k^*$ . (b)  $S_k^\pm$  represents the asymptotic soliton associated with  $\lambda_k$  as  $z \rightarrow \pm\infty$ . (c)  $S_{k1}^\pm$  and  $S_{k2}^\pm$  denote a pair of asymptotic solitons corresponding to  $\lambda_k$  in the resonant interaction as  $z \rightarrow \pm\infty$ .

*Anti-dark and Mexican-hat solitons.* — With  $N = 1$ , the once-iterated solution can describe both the AD and Mexican-hat (MH) solitons on top of the CW background if  $\mu_1^{(1)} = 0$ , but only the AD soliton if either  $\mu_1^{(2)} = 0$  or  $\mu_1^{(3)} = 0$ .

In the case  $\mu_1^{(1)} = 0$  (i.e.,  $\alpha_1 \beta_1^* - \beta_1 \alpha_1^* = 0$ ), the solution can be written as

$$u = -\rho e^{i\left(\frac{t}{6\varepsilon} - \frac{z}{108\varepsilon^2} + \phi\right)} - \frac{\sqrt{2} \chi_1^2 e^{i\left(\frac{t}{6\varepsilon} - \frac{z}{108\varepsilon^2} + \phi\right)}}{\sqrt{2} \rho + |\lambda_1| e^{i[\text{Arg}(\alpha_1) - \text{Arg}(\beta_1)]} \cosh \left[ 2\theta_1(t, z) + \frac{1}{2} \ln \left( \frac{|\alpha_1|^2 \chi_1^-}{|\beta_1|^2 \chi_1^+} \right) \right]}, \quad (7)$$

whose intensity displays two different profiles depending on the arguments of  $\alpha_1$  and  $\beta_1$ . With  $\text{Arg}(\alpha_1) = \text{Arg}(\beta_1)$ , solution (7) represents the bell-shaped AD soliton as shown in Fig. 1. The maximum intensity, soliton velocity and width can be characterized by  $|u|_{\max}^2 = \frac{[\rho|\lambda_1| + \sqrt{2}(\rho^2 - \lambda_1^2)]^2}{(|\lambda_1| - \sqrt{2}\rho)^2}$  and  $w = \frac{1}{2\chi_1}$ , respectively. If  $\text{Arg}(\alpha_1) = \text{Arg}(\beta_1) + \pi$ , solution (7) exhibits that one hump is symmetrically accompanied with two dips beneath the CW background, which looks like the Mexican-hat shape [24] (also seen in Fig. 1). The velocity and width of the MH soliton are the same as those of the AD one, but its intensity drastically increases to  $|u|_{\max}^2 = \frac{[\rho|\lambda_1| + \sqrt{2}(\lambda_1^2 - \rho^2)]^2}{(|\lambda_1| + \sqrt{2}\rho)^2}$  at the center of the hump, and drops to zero at the centers of two dips. Our calculation shows that associated with the same  $\lambda_1$ , the area of the AD soliton is exactly equivalent to that of the hump of the MH soliton subtracting off two dips. Therefore, the generation of the MH soliton could be ascribed to that the transfer of some energy from the CW background to the AD soliton causes the rising of the hump and two dips sinking in the CW background.

*Resonant and elastic interactions.* — For the generic case  $\mu_1^{(i)} \neq 0$  ( $1 \leq i \leq 3$ ) of the once-iterated solution, our asymptotic analysis indicates that there are three solitons in total as  $z \rightarrow \pm\infty$  (the detailed expressions of the asymptotic solitons are omitted for saving the space), and their wave numbers and frequencies exactly satisfy the resonant condition. Associated with  $\lambda_1 > 0$  and  $\lambda_1 < 0$ , Figs. 2 and 3 respectively demonstrate the three-soliton resonant structure of two solitons merging into one soliton:  $(S_{11}^-, S_{12}^-) \rightarrow S_1^+$ , and the structure of one soliton diverging into two solitons:  $S_1^- \rightarrow (S_{11}^+, S_{12}^+)$ . The occurrence of such resonant phenomena is related to the modulation instability of the seed solution  $u = \rho e^{i(\frac{t}{6\varepsilon} - \frac{z}{108\varepsilon^2} + \phi)}$ . It has been predicted that the resonant interaction for the exciting wave created from a CW background possibly takes place in the centro-symmetric single-mode optical fiber around zero-dispersion region [25].

By implementing the DT two times, one can derive the two-soliton solution under the condition  $\mu_k^{(i)} = \mu_{3-k}^{(j)} = 0$  ( $1 \leq i, j \leq 3$ ) for some  $1 \leq k \leq 2$ . In this case, the solution describes that the elastic interaction can occur between two AD solitons, or two MH solitons, or the AD and MH solitons. For example, Figs. 4 and 5 illustrate that the MH soliton can completely recover its shape, velocity and intensity after interacting with the AD or MH soliton, which suggests that the MH soliton admits the elastic interaction on the CW background.

Besides, we observe an unusual phenomenon in both the resonant and elastic soliton interactions, that is, the CW background may exchange its energy with the AD or MH soliton under proper

choice of the parameters. Such energy exchange leads to that some AD soliton changes into an MH one or some MH soliton into an AD one upon an interaction. For illustrative purpose, Fig. 6 shows that in the divergent resonance  $S_1^- \rightarrow (S_{11}^+, S_{12}^+)$ , the outgoing soliton  $S_{12}^+$  acquires the energy from the background and forms an MH soliton; Fig. 7 displays that upon an elastic interaction with one AD soliton, the MH soliton  $S_2^-$  transfers its energy to the background and becomes an AD soliton  $S_2^+$ .

*Various combinations of resonant and elastic interactions.* — Since both the resonant and elastic interactions are coexistent in Eq. (1), one can further obtain more complicated, abundant soliton interactions which are comprised of such two fundamental interactions. That implies that the number, velocities and intensities of the incoming solitons are in general different from those of the outgoing ones. In what follows, we take the twice-iterated solution as an example to discuss the following two cases:

- (1) If only one of  $\mu_k^{(i)}$ 's ( $1 \leq i \leq 3, 1 \leq k \leq 2$ ) is equal to 0, the solution can exhibit the elastic-confluent and elastic-divergent interaction patterns (which are both the partially inelastic interactions) associated with  $\lambda_{k-3} > 0$  and  $\lambda_{k-3} < 0$ , respectively. In illustration, Fig. 8 shows that two incoming solitons  $S_{11}^-$  and  $S_{12}^-$  merge into one outgoing soliton  $S_1^+$  via a confluent resonant interaction, while the physical quantities of the incoming soliton  $S_2^-$  keep the same as those of the outgoing one  $S_2^+$ ; Fig. 9 presents that one incoming soliton  $S_2^-$  diverges into two outgoing ones  $S_{21}^+$  and  $S_{22}^+$  via a divergent resonant interaction, while the other incoming soliton  $S_1^-$  retains its amplitude, velocity and energy before and after interaction.
- (2) If none of  $\mu_k^{(i)}$ 's ( $1 \leq i \leq 3, 1 \leq k \leq 2$ ) equals to 0, the solution can display three kinds of completely inelastic interaction patterns: the confluent-divergent, confluent-confluent, divergent-divergent combinations, which correspond to  $\lambda_1 \lambda_2 < 0$ ,  $\lambda_1, \lambda_2 > 0$  and  $\lambda_1, \lambda_2 < 0$ , respectively. Fig. 10 gives the confluent-divergent interaction in which two incoming solitons  $S_{11}^-$  and  $S_{12}^-$  merge into one outgoing soliton  $S_1^+$ , and one incoming soliton  $S_2^-$  diverges into two outgoing ones  $S_{21}^+$  and  $S_{22}^+$ . As shown in Figs. 11 and 12, one can see that the confluent-confluent and divergent-divergent interactions are respectively comprised of a pair of confluent resonance  $[(S_{11}^-, S_{12}^-) \rightarrow S_1^+ \text{ and } (S_{21}^-, S_{22}^-) \rightarrow S_2^+]$ , and a pair of divergent resonance  $[S_1^- \rightarrow (S_{11}^+, S_{12}^+)$  and  $S_2^- \rightarrow (S_{21}^+, S_{22}^+)]$ .

*Conclusion.* — Using the successively-iterated DT algorithm and starting from a nonzero seed, we have constructed a general family of soliton solutions for Eq. (1), which can be uniformly represented in terms of a multi-component determinant. We have shown that the once-iterated solution can represent the AD or MH soliton on a CW background with suitable parametric condition. By the asymptotic analysis of the twice-iterated solution, we have further revealed that Eq. (1) admits not only the resonant and elastic interactions, but various partially/completely inelastic interactions comprised of such two fundamental interactions. In addition, we have found that upon an interaction the energy exchange may take place between some interacting soliton and the background, which can cause the change of an AD soliton into an MH one, or an MH soliton into an AD one. These results enrich our understanding of the soliton interactions in the (1+1)-DIEs with a single field. Since Eq. (1) has arisen from optical fibers, we expect that these novel soliton interaction phenomena will be observed in the near future experiments, and bring about some applications in all-optical information processing, optical switching, and routing of optical signals [26].

This work has been supported by the Science Foundations of China University of Petroleum, Beijing (Grant No. BJ-2011-04), by the Special Funds of the National Natural Science Foundation of China (Grant No. 11247267), and by the National Natural Science Foundations of China under Grant No. 11371371. ML is grateful for the support by the Fundamental Research Funds of the Central Universities (Project No. 2014QN30).

## References

- [1] G. Biondini and Y. Kodama, *J. Phys. A* **36** 10519 (2003).
- [2] G. Biondini and S. Chakravarty, *J. Math. Phys.* **47**, 033514 (2006).
- [3] S. Chakravarty and Y. Kodama, *J. Phys. A* **41**, 275209 (2008); *Stud. Appl. Math.* **123**, 83 (2009).
- [4] M. J. Ablowitz and P. A. Clarkson, *Solitons, Nonlinear Evolution Equations and Inverse Scattering* (Cambridge Univ. Press, Cambridge, 1992).
- [5] N. Sasa and J. Satsuma, *J. Phys. Soc. Jpn.* **60**, 409 (1991).

- [6] Y. Kodama, J. Stat. Phys. **39**, 597 (1985); Y. Kodama and A. Hasegawa, IEEE J. Quantum Electron. **23**, 510 (1987).
- [7] D. Mihalache, L. Torner, F. Moldoveanu, N.-C. Panoiu, and N. Truta, Phys. Rev. E **48**, 4699 (1993); J. Phys. A **26**, L757 (1993).
- [8] C. Gilson, J. Hietarinta, J. Nimmo, and Y. Ohta, Phys. Rev. E **68**, 016614 (2003).
- [9] D. Mihalache, N. Truta, and L. C. Crasovan, Phys. Rev. E **56**, 1064 (1997).
- [10] J. Kim, Q. H. Park, and H. J. Shin, Phys. Rev. E **58**, 6746 (1998).
- [11] A. Sergyeyev and D. Demskoi, J. Math. Phys. **48**, 042702 (2007).
- [12] J. K. Yang and D. J. Kaup, J. Math. Phys. **50**, 023504 (2009).
- [13] O. C. Wright III, Chaos Solitons Fractals **33**, 374 (2007).
- [14] Y. S. Li and W. T. Han, Chin. Ann. Math. Ser. B **22**, 171 (2001).
- [15] T. Xu and X. M. Xu, Phys. Rev. E **87**, 032913 (2013); T. Xu, D. H. Wang, M. Li, and H. Liang, Phys. Scr. **89**, 075207 (2014).
- [16] K. Porsezian and K. Nakkeeran, Phys. Rev. Lett. **76**, 3955 (1996); M. Gedalin, T. C. Scott, and Y. B. Band, Phys. Rev. Lett. **78**, 448 (1997).
- [17] Z. H. Li, L. Li, H. P. Tian, and G. S. Zhou, Phys. Rev. Lett. **84**, 4096 (2000).
- [18] Y. Jiang and B. Tian, EPL **102**, 10010 (2013).
- [19] Y. Ohta, AIP Conference Proceedings **1212**, 114 (2010).
- [20] U. Bandelow and N. Akhmediev, Phys. Rev. E **86**, 026606 (2012); S. H. Chen, Phys. Rev. E **88**, 023202 (2013).
- [21] L. C. Zhao, S. C. Li, and L. M. Ling, Phys. Rev. E **89**, 023210 (2014).
- [22] V. B. Matveev and M. A. Salle, *Darboux Transformations and Solitons* (Springer Press, Berlin, 1991).



- [23] T. Xu and B. Tian, *J. Math. Phys.* **51**, 033504 (2010); T. Xu, B. Tian, Y. S. Xue, and F. H. Qi, *EPL* **92**, 50002 (2010).
- [24] In our opinion, the term “Mexican-hat soliton” is more accurate than the term “W-shaped soliton” because the center of the hump is far above the background. Note that the double-hole dark soliton also has the “W” shape but the hump’s center is beneath the background [18, 19].
- [25] W. N. Cui and G. X. Huang, *Chin. Phys. Lett.* **21**, 2437 (2004).
- [26] G. P. Agrawal, *Nonlinear Fiber Optics* (5th edition, Academic, Oxford, 2012).

## Figures and captions

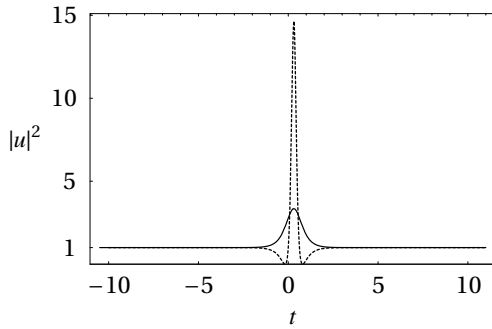


Figure 1: AD and MH solitons via solution (7) transverse at  $z = 0$ , where  $|\alpha_1| = |\beta_1| = 1$ ,  $\rho = 1$ ,  $\lambda_1 = 2$ ,  $\phi = 1$  and  $\varepsilon = 0.1$ . Solid line for the AD soliton with  $\text{Arg}(\alpha_1) = \text{Arg}(\beta_1)$ , and dashed line for the MH soliton with  $\text{Arg}(\alpha_1) = \text{Arg}(\beta_1) + \pi$ .

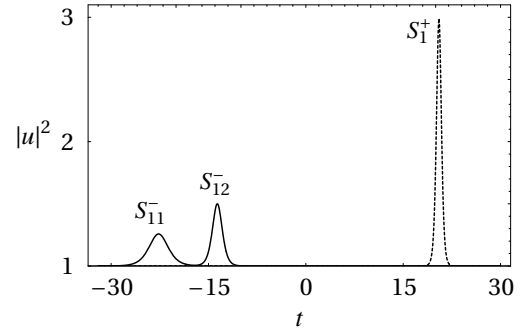


Figure 2: Confluent-resonant interaction of three AD solitons with  $\alpha_1 = 1$ ,  $\beta_1 = 1 + i$ ,  $\gamma_1 = 1 + 2i$ ,  $\rho = 1$ ,  $\lambda_1 = \frac{3}{2}$ ,  $\phi = 0$  and  $\varepsilon = 0.2$ . Solid line:  $z = -8$ ; Dashed line:  $z = 8$ .

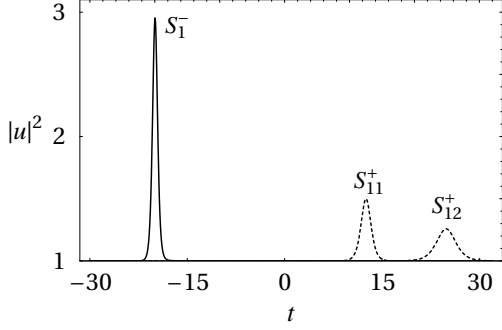


Figure 3: Divergent-resonant interaction of three AD solitons with the same parameters as those in Fig. 2 except for  $\lambda_1 = -\frac{3}{2}$ . Solid line:  $z = -8$ ; Dashed line:  $z = 8$ .

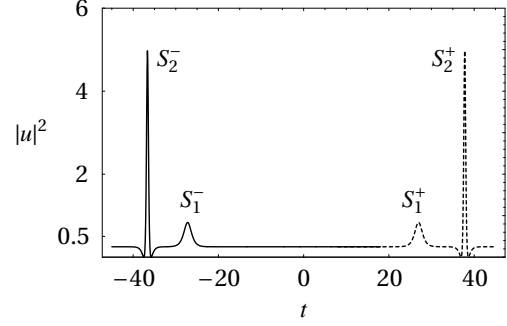


Figure 4: Elastic interaction between the AD and MH solitons with  $\alpha_1 = \alpha_2 = 1$ ,  $\beta_1 = 2$ ,  $\beta_2 = 1$ ,  $\gamma_1 = 1$ ,  $\gamma_2 = 1 + i$ ,  $\rho = 1/2$ ,  $\lambda_1 = -1$ ,  $\lambda_2 = \frac{\sqrt{6}}{2}$ ,  $\phi = 0$  and  $\varepsilon = 0.2$ . Solid line:  $z = -20$ ; Dashed line:  $z = 20$ .

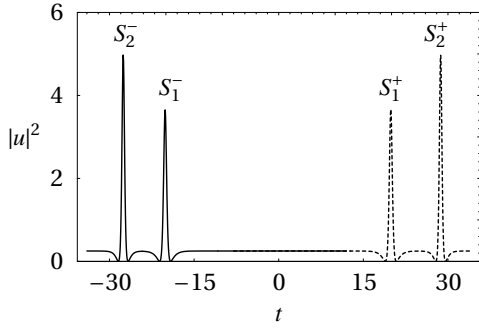


Figure 5: Elastic interaction between two MH solitons with the same parameters as those in Fig. 4 except for  $\beta_1 = -2$ . Solid line:  $z = -15$ ; Dashed line:  $z = 15$ .

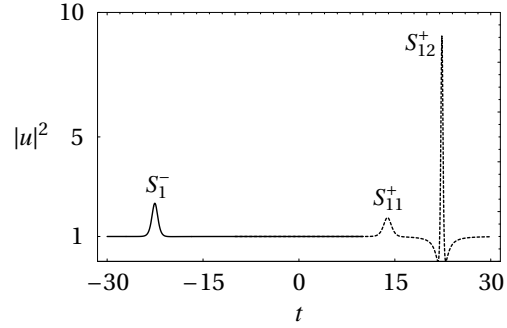


Figure 6: Change of an AD soliton into a MH soliton in the resonant interaction, where the parameters are the same as those in Fig. 2 except that  $\lambda_1 = -\sqrt{2} - 0.01$  and  $\gamma_1 = 1 - 2i$ . Solid line:  $z = -10$ ; Dashed line:  $z = 8$ .

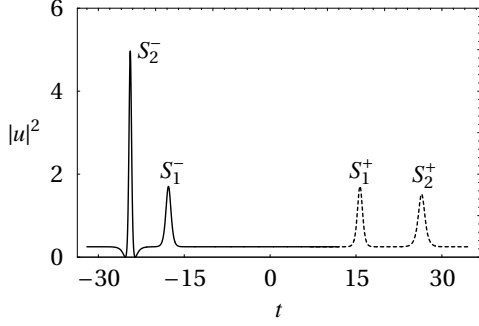


Figure 7: Change of a MH soliton into an AD soliton in the elastic interaction, where the parameters are the same as those in Fig. 4 except that  $\beta_1 = i$ ,  $\beta_2 = -1$ ,  $\gamma_2 = 1 - i$  and  $\varepsilon = 0.25$ . Solid line:  $z = -12$ ; Dashed line:  $z = 12$ .

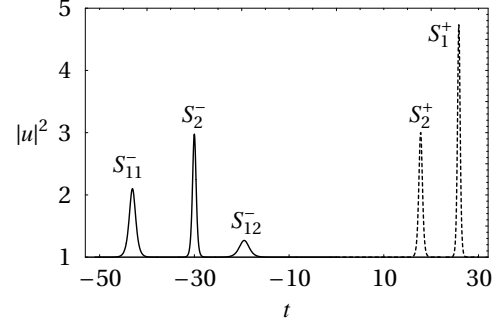


Figure 8: Elastic-confluent interaction of the AD solitons with  $\alpha_1 = \alpha_2 = 1$ ,  $\beta_1 = 1 + i$ ,  $\beta_2 = i$ ,  $\gamma_1 = \gamma_2 = 1$ ,  $\rho = 1$ ,  $\phi = 0$ ,  $\lambda_1 = \sqrt{3}$ ,  $\lambda_2 = -\frac{3}{2}$  and  $\varepsilon = 0.2$ . Solid line:  $z = -12$ ; Dashed line:  $z = 8$ .

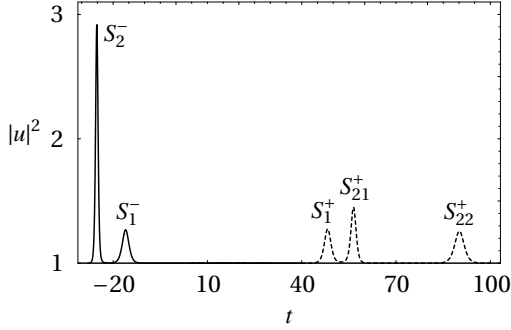


Figure 9: Elastic-divergent interaction of the AD solitons with the same parameters as those in Fig. 8 except that  $\beta_1 = i$  and  $\beta_2 = 1 + i$ . Solid line:  $z = -10$ ; Dashed line:  $z = 30$ .

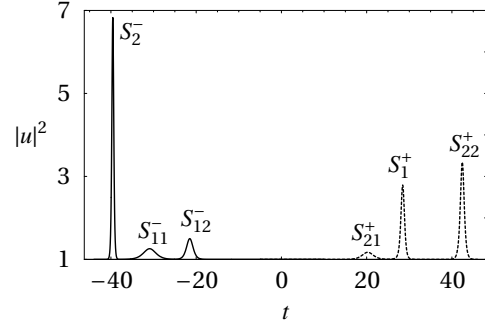


Figure 10: Confluent-divergent interaction of the AD solitons with  $\alpha_1 = \alpha_2 = 1$ ,  $\beta_1 = 1 + i$ ,  $\beta_2 = 2 + i$ ,  $\gamma_1 = \gamma_2 = 1$ ,  $\rho = 1$ ,  $\lambda_1 = \frac{3}{2}$ ,  $\lambda_2 = -2$ ,  $\phi = 0$  and  $\varepsilon = 0.1$ . Solid line:  $z = -15$ ; Dashed line:  $z = 15$ .

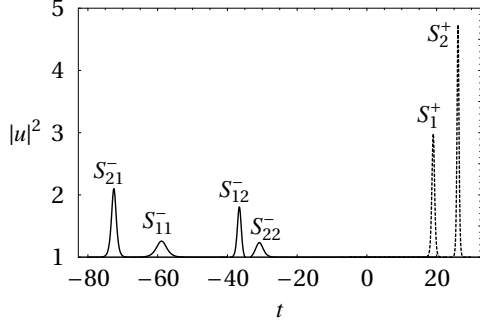


Figure 11: Confluent-confluent interaction of the AD solitons with  $\alpha_1 = \alpha_2 = 1$ ,  $\beta_1 = \beta_2 = i$ ,  $\gamma_1 = 1 + i$ ,  $\gamma_2 = 1 - i$ ,  $\rho = 1$ ,  $\lambda_1 = \frac{3}{2}$ ,  $\lambda_2 = \sqrt{3}$ ,  $\phi = 0$  and  $\varepsilon = 0.2$ . Solid line:  $z = -20$ ; Dashed line:  $z = 8$ .

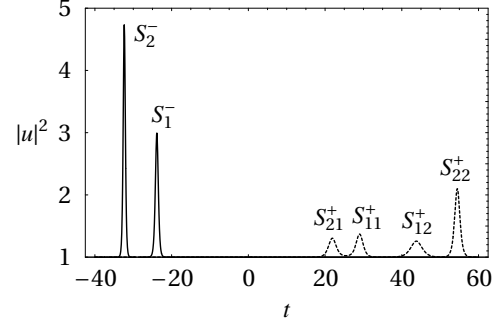


Figure 12: Divergent-divergent interaction of the AD solitons with the same parameters as those in Fig. 11 except that  $\lambda_1 = -\frac{3}{2}$  and  $\lambda_2 = -\sqrt{3}$ . Solid line:  $z = -10$ ; Dashed line:  $z = 15$ .